DALTON
FULL PAPER

Unique structural and physical properties of $Ni(dmit)_2$ anion radical salts characterized by short Te · · · S contacts (dmit = 1,3-dithiole-2-thione-4,5-dithiolate)

Masahiro Fujiwara [a] **and Reizo Kato** *[b]

[a] *The Institute for Solid State Physics, The University of Tokyo, 5-1-5 Kashiwanoha, Kashiwa-shi, Chiba 277-8581, Japan. E-mail: mfuji@issp.u-tokyo.ac.jp*
[b] *RIKEN, 2-1 Hirosawa, Wako-shi, Saitama 351-0198, Japan. E-mail: reizo@postman.riken.go.jp*

Received 19th April 2002, Accepted 1st August 2002
First published as an Advance Article on the web 12th September 2002

Five new $Ni(dmit)_2$ anion radical salts, $[Me_3Te][Ni(dmit)_2]_2$ (**1**), $[Me_3Te][Ni(dmit)_2]_3 \cdot (CH_3)_2C(O)$ (**2**), α-[MOT][Ni(dmit)$_2$]$_2$ (**3**), β-[MOT][Ni(dmit)$_2$]$_2$ (**4**), and γ-[MOT][Ni(dmit)$_2$]$_2$ (**5**) (dmit = 1,3-dithiole-2-thione-4,5-dithiolate; MOT = 1-oxa-4-methyl-4-telluracyclohexane) have been prepared by galvanostatic electrolysis. X-Ray crystal structure analyses show that all the salts are characterized by short Te · · · S contacts (3.41–3.85 Å) between the anions and cations. Each salt shows unique molecular packing of the $Ni(dmit)_2$ units. The electronic structures are strongly dependent on these unique molecular arrangements. Among them, **1** and **3** show metallic behavior (down to 60 and 160 K, respectively) and the resistivity of **4** is almost independent of temperature, increasing moderately below 40 K.

Introduction

To date, there has been considerable interest in 1,2-dithiolene complexes that possess unusual electronic and magnetic properties. Among them, studies on $Ni(dmit)_2$ anion radical salts[1] have been extended to various categories of materials, such as electrical conductors, including Langmuir–Blodgett films,[2] molecular magnets,[3] and nonlinear optical materials.[4]

The $M(dmit)_2$ (M = Ni, Pd) complex has planar geometry and ten peripheral S atoms (see Scheme 1). These ten S atoms

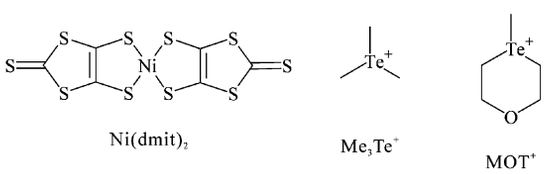

Scheme 1

lead to the formation of two- or three-dimensional S · · · S networks in crystals. The differences between the $Ni(dmit)_2$ and $Pd(dmit)_2$ salts are down to the degree of dimerization in the solid state. The $Ni(dmit)_2$ molecule has less of a tendency to form a dimer unit, while most $Pd(dmit)_2$ salts contain strongly dimerized $Pd(dmit)_2$ units associated *via* effective Pd · · · Pd contacts. This affords the $Ni(dmit)_2$ molecule more degrees of freedom for the molecular arrangement and orientation. $Ni(dmit)_2$ salts with open- or closed-shell cations show a variety of crystal structures and various formal charges of the anion radical.[5] However, investigations focused on the correlation between molecular arrangement and physical properties for the $Ni(dmit)_2$ system remain restricted in scope. This article is devoted to the development of crystal designs with improved conducting properties for the $Ni(dmit)_2$ system.

The electronic structures of the $M(dmit)_2$-based molecular conductors strongly depend on the central metal. The conduction band of the $Ni(dmit)_2$ system originates from the LUMO, while that of the $Pd(dmit)_2$ system originates from the HOMO.[6] This difference is also due to the degree of the dimerization. For an ideal $M(dmit)_2$ molecule with D_{2h} symmetry, the LUMO has b_{2g} symmetry while the HOMO has a_{2u} symmetry. b_{2g} LUMO symmetry, where the sign of the wave function changes at the central metal atom, is not suitable for enhancement of the intermolecular interaction in the sideways direction. This is because the antisymmetric character of the LUMO effectively reduces the side-by-side interaction, which is determined mainly by the sum of the S · · · S overlap integrals. Therefore, the $Ni(dmit)_2$ system tends to have a one-dimensional conduction band, which leads to an unstable metallic state at low temperatures.[7] When dimerization is present and strongly correlated electrons exist in the $Ni(dmit)_2$ salts, another factor reduces the stability of the metallic state. Dimerization generates upper (antibonding) and lower (bonding) LUMO bands separated by an energy gap. In the system with the frequently observed formal charge of −1/2, the lower LUMO band is half-filled. If the intradimer Coulomb interaction is much larger than the band width, the system behaves as a Mott insulator.[8]

One possible molecular arrangement which avoids these situations was found in α-$[Et_2Me_2N][Ni(dmit)_2]_2$, which is metallic down to very low temperatures.[9] In this compound, one $Ni(dmit)_2$ molecule overlaps with two neighboring molecules within the face-to-face stacking. This 'spanning overlap' mode enables a two-dimensional conduction band to be formed.

We report here that the 'chalcogen · · · chalcogen contact' found characteristically between the Te-containing cation and the dmit ligand suggests another route towards improved conducting properties. The closed-shell counter cations in the anion radical salts do not form the conduction band, but their size, shape, and charge often have a significant influence on the crystal structures and, thus, the physical properties. Introduction of strong and directional donor · · · anion interactions has been found to be effective in the regulation of molecular arrangement and orientation in conducting cation radical salts.[10] No successful example, however, is yet known in anion radical salts. In this context, the use of Te-containing cations is of special interest. The Te atom has a strong tendency to form intermolecular interactions called 'secondary bonds' in crystal-

DOI: 10.1039/b203834j

line compounds.[11] We have used the tellurium-based secondary bond to form supramolecular donor ··· anion interactions in anion radical salts. All the $Ni(dmit)_2$ salts with trialkyltelluronium ions of trigonal pyramidal geometry exhibit Te ··· S interactions which play a significant role in determining the molecular arrangement and, consequently, the electronic structure.

Experimental

Syntheses

All syntheses were carried out under Ar atmosphere. $Me_3Te{\cdot}I$, 1-oxa-4-methyl-4-telluracyclohexane iodide (abbreviated as MOT·I) and $[Bu^n_4N][Ni(dmit)_2]$ were synthesized by the literature methods.[12,13] Other reagents were purchased and used as received.

$Me_3Te{\cdot}ClO_4$. To a methanol solution (300 ml) of $Me_3Te{\cdot}I$ (1.500 g, 5.00 mmol) was added a methanol solution (30 ml) of $Ag{\cdot}ClO_4$ (1.036 g, 5.00 mmol), dropwise. The reaction mixture was stirred at room temperature for 3 h. After the resultant lemon yellow precipitate was filtered off, the solvent was evaporated *in vacuo* to afford the crude product. Recrystallization from MeOH–Et_2O (three times) afforded pure $Me_3Te{\cdot}ClO_4$ (780 mg, 2.86 mmol) as colorless plates in 57% yield. Anal. calcd for $C_3H_9ClO_4Te$: C, 13.24; H, 3.33; O, 23.51; found: C, 13.32; H, 3.39; O, 23.43%.

MOT·ClO_4. The method basically followed previous literature reports.[11] To a methanol solution (150 ml) of MOT·I (1.864 g, 5.45 mmol) was added a methanol solution (30 ml) of $Ag{\cdot}ClO_4$ (1.129 g, 5.45 mmol), dropwise. The reaction mixture was stirred at room temperature overnight. After the resultant lemon yellow precipitate was filtered off, the solvent was evaporated *in vacuo* to afford the crude product. Recrystallization from MeOH–Et_2O (three times) afforded pure MOT·ClO_4 (1.276 g, 4.06 mmol) as colorless plates in 74% yield. Anal. calcd for $C_5H_{11}ClO_5Te$: C, 19.11; H, 3.53; O, 25.46; found: C, 19.21; H, 3.39; O, 25.18%.

Preparation of anion radical salts. Single crystals of $[Me_3Te][Ni(dmit)_2]_2$ (**1**), $[Me_3Te][Ni(dmit)_2]_3{\cdot}(CH_3)_2C(O)$ (**2**), *α*-$[MOT][Ni(dmit)_2]_2$ (**3**), *β*-$[MOT][Ni(dmit)_2]_2$ (**4**), and *γ*-$[MOT][Ni(dmit)_2]_2$ (**5**) were obtained by galvanostatic electrolysis of a mixture of $[Bu^n_4N][Ni(dmit)_2]$ (10–15 mg) and a large excess of the ClO_4 salt of the corresponding telluronium ion as supporting electrolyte (70–120 mg) in 20 ml of acetone or a mixture of acetone and acetonitrile (1:1, v/v) under Ar. An H-shaped 20 ml cell and Pt electrodes (1 mm diameter) were used and a constant current of 0.5 μA was applied for several weeks at 20 °C.

X-Ray crystallography

Intensity data at room temperature were collected on an automatic four-circle diffractometer (Rigaku, AFC-7R) or an imaging plate (MAC Science, DIP320S) equipped with a rotating anode and graphite-monochromated Mo-Kα radiation (λ = 0.71070 Å). The unit cell parameters were determined by least-squares refinements on the basis of the setting angles of 25 reflections measured by the four-circle diffractometer. The intensities in the four-circle diffractometer measurements were corrected for Lorentz and polarization effects. The structures were solved by a direct method using SIR97 and refined by a full-matrix least-squares method. When the four-circle diffractometer was used, analytical absorption correction was also carried out. In the case of the imaging plate, the absorption correction was included in the scaling process of the image data and an absorption correction based on DIFABS[14] was applied to each data set. Anisotropic thermal parameters were used for non-hydrogen atoms, except for special indications. All hydrogen atoms were added in calculated positions with fixed isotropic contributions. For **5**, the refinement was performed using SHELXL-97.[15] For others, calculations were performed using the teXsan crystallographic software package (Molecular Structure Corp., The Woodlands, TX, USA, 1985 and 1992)

$[Me_3Te][Ni(dmit)_2]_2$ (1). $C_{15}H_9Ni_2S_{20}Te$, space group $P\bar{1}$, a = 7.473(2), b = 36.11(1), c = 6.482(2) Å, α = 92.49(8), β = 110.4(1), γ = 95.36(4)°, V = 1626(1) Å,^{3} Z = 2, and D_{calcd} = 2.196 g cm^{-3}. A plate-like crystal of dimensions 0.50 × 0.12 × 0.03 mm^3 was used. Intensity data (4193 unique reflections, $2\theta \leq 57.7°$) were collected, and 2827 reflections with $I > 3\sigma(I)$ were used in the calculation. The final R and R_w are 0.041 and 0.054, respectively.

$[Me_3Te][Ni(dmit)_2]_3{\cdot}(CH_3)_2C(O)$ (2). $C_{24}H_{15}ONi_3S_{30}Te$, space group $P2_1/n$, a = 38.01(2), b = 11.955(2), c = 11.173(2) Å, β = 90.2(1)°, V = 5077(3) Å^3, Z = 4, and D_{calcd} = 2.073 g cm^{-3}. An elongated plate-like crystal of dimensions 0.80 × 0.20 × 0.03 mm^3 was used. Intensity data (6854 unique reflections, $2\theta \leq 56.5°$) were collected, and 3163 reflections with $I > 3\sigma(I)$ were used in the calculation. Heavy atoms were refined anisotropically and the C and H atoms in the cation were refined isotropically. The final R and R_w are 0.041 and 0.049, respectively.

***α*-[MOT][Ni(dmit)$_2$]$_2$ (3).** $C_{17}H_{11}ONi_2S_{20}Te$, space group $P2_1/c$, a = 37.695(7), b = 7.097(1), c = 12.589(2) Å, β = 92.846(4)°, V = 3363(1) Å^3, Z = 4, and D_{calcd} = 2.207 g cm^{-3}. A needle-shaped crystal of dimensions 0.40 × 0.05 × 0.05 mm^3 was used. Intensity data (4075 unique reflections, $2\theta \leq 61.0°$) were collected by the ω scan technique, and 1627 reflections with $I > 3\sigma(I)$ were used in the calculation. The Ni and S atoms were refined anisotropically and the C, H, and O atoms in the cation isotropically. The final R and R_w are 0.079 and 0.113, respectively.

***β*-[MOT][Ni(dmit)$_2$]$_2$ (4).** $C_{17}H_{11}ONi_2S_{20}Te$, space group $P2_1/n$, a = 12.093(6), b = 37.163(9), c = 7.716(7) Å, β = 105.51(5)°, V = 3341(3) Å^3, Z = 4, and D_{calcd} = 2.221 g cm^{-3}. A needle-shaped crystal of dimensions 0.25 × 0.03 × 0.02 mm^3 was used. Intensity data (5076 unique reflections, $2\theta \leq 56.7°$) were collected, and 2485 reflections with $I > 3\sigma(I)$ were used in the calculation. The H and O atoms in the cation were refined isotropically and all other atoms were refined anisotropically. The final R and R_w are 0.081 and 0.126, respectively.

***γ*-[MOT][Ni(dmit)$_2$]$_2$ (5).** $C_{17}H_{11}ONi_2S_{20}Te$, $P\bar{1}$, a = 11.786(5), b = 19.266(4), c = 7.548(2) Å, α = 92.54(2), β = 101.78(2), γ = 82.06(2)°, V = 1661.6(9) Å^3, Z = 2, and D_{calcd} = 2.233 g cm^{-3}. An elongated plate-like crystal of dimensions 0.68 × 0.22 × 0.04 mm^3 was used. Intensity data (9696 unique reflections, $2\theta \leq 60.0°$) were collected by the ω scan technique, and 7587 reflections with $I > 3\sigma(I)$ were used in the calculation. All non-hydrogen atoms were refined anisotropically and the H atoms of the cation were refined isotropically. The difference Fourier synthesis shows an additional small peak that suggests weak (conformational) disorder of the Te atom in the cation. The refinement of site occupancies, however, was unsuccessful. The final R and R_w are 0.042 and 0.163, respectively.

CCDC reference numbers 184206–184210.

See http://www.rsc.org/suppdata/dt/b2/b203834j/ for crystallographic data in CIF or other electronic format.

Resistivity measurements

The d.c. resistivity measurements were performed using the standard four-probe method. Electrical contacts were obtained by gluing four gold wires (10 or 15 μm diameter) to the crystal with gold paste.

Table 1 Exponents ζ and the ionization potentials I_p (Ryd.) for the atomic orbitals

	Ni			S		C	
	4s	4p	3d	3s	3p	2s	2p
ζ	2.100	2.100		2.122	1.827	1.625	1.625
Double-ζ			5.750 (0.5798) 2.300 (0.5782)				
$-I_p$ (Ryd.)	0.805	0.461	1.044	1.620	0.770	1.573	0.838

Band calculations

The LUMO was obtained by extended Hückel MO calculation.[16] The calculation was carried out with the use of semi-emperical parameters for Slater-type atomic orbitals (Table 1). Double-ζ orbitals were used for Ni. Band calculations were performed under the tight-binding approximation.[17] Transfer integrals (t) were approximated from overlap integrals (S) *via* the formula $t \cong \varepsilon S$ (ε is a constant whose order is the one of the energy level of the LUMO: $\varepsilon = -10$ eV). Because there is an interlayer interaction in every salt examined, three-dimensional band calculations were carried out.

Results and discussion

Preparation of $Ni(dmit)_2$ salts with trialkyltelluroniums

$[Me_3Te][Ni(dmit)_2]_2$ (**1**), $[Me_3Te][Ni(dmit)_2]_3{\cdot}(CH_3)_2C(O)$ (**2**), α-, β-, and γ-$[MOT][Ni(dmit)_2]_2$ (**3**, **4**, and **5**) were obtained by galvanostatic electrolysis of a mixture of $[Bu^n_4N][Ni(dmit)_2]$ with large excess of the ClO_4^- salt of the corresponding telluronium ion as the supporting electrolyte. We tried to prepare single crystals by electrochemical oxidation of a mixture of the monovalent $Ni(dmit)_2$ salts of the corresponding telluronium ion and the supporting electrolyte, but single crystals of sufficient quality for crystal structure analysis could not be obtained.

From the solution containing $[Ni(dmit)_2]^-$ and Me_3Te^+, three different kinds of anion radical salts, $[Me_3Te][Ni(dmit)_2]_2$ (**1**), $[Me_3Te][Ni(dmit)_2]_3{\cdot}(CH_3)_2C(O)$ (**2**), and some unidentified black plates, were obtained. The major product was **2** or the third salt, whose cation:anion ratio was determined to be 1:2 by energy dispersive X-ray spectroscopy (EDS). The crystal structure of this 1:2 salt has not been determined yet because of the low quality of the crystals. This salt shows a low resistivity value at room temperature ($\rho_{r.t.} = 20\ \Omega$ cm), but semiconducting behavior with a large activation energy value ($E_a = 0.2$ eV).

Polymorphism was detected in the MOT^+ salt. From the $[Ni(dmit)_2]^-$–MOT^+ solution, three phases of $[MOT][Ni(dmit)_2]_2$ (**3**: plates, **4**: rods, **5**: blocks) were obtained as high quality crystals. The major product was **5**.

Crystal and electronic structures of $[Me_3Te][Ni(dmit)_2]_2$ (1)

The crystal structure of $[Me_3Te][Ni(dmit)_2]_2$ (**1**) is shown in Fig. 1. This salt belongs to the triclinic system with the space group $P\bar{1}$. The $Ni(dmit)_2$ layers and the cation layers are arranged alternately along the b axis. The unit cell contains two crystallographically independent $Ni(dmit)_2$ columns, each of which forms a conduction layer through intermolecular S ⋯ S contacts. The $Ni(dmit)_2$ units exhibit the '*solid-crossing*' column structure, where the $Ni(dmit)_2$ units stack along the [101] direction in Layer I and along the [100] direction in Layer II. These two layers differ from each other in their stacking modes (*vide infra*).

The distinctive feature of this salt is existence of three short Te ⋯ S contacts between the cations and the $Ni(dmit)_2$ units. The Te atom in the Me_3Te^+ cation has one short contact with Layer I (3.79 Å) and two contacts with Layer II (3.66 Å) (Fig. 2). Considering that the sum of the van der Waals radii is 3.90 Å, these Te ⋯ S contacts are rather short. On Layer II,

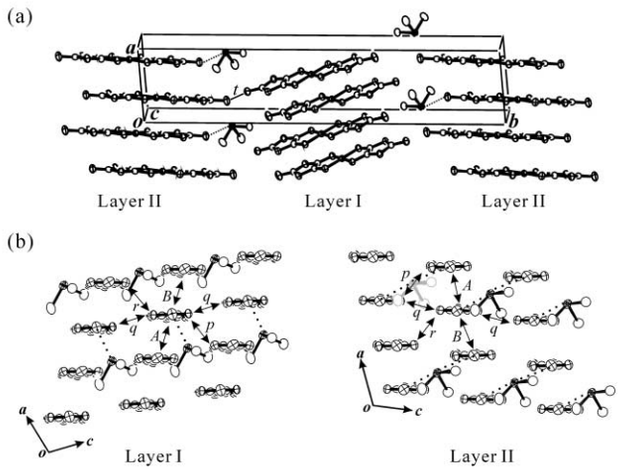

Fig. 1 Crystal structure of $[Me_3Te][Ni(dmit)_2]_2$ **1**: (a) side view and (b) end-on projection.

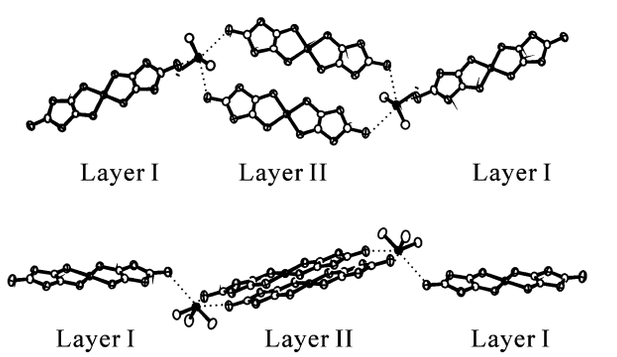

Fig. 2 Top view (upper) and side view (lower) of short Te ⋯ S contacts in **1**.

the Te atom bridges adjacent $Ni(dmit)_2$ units aligned along the [101] direction [Fig. 1(b) and 2]. This Te atom additionally contacts one thioxo sulfur atom of the $Ni(dmit)_2$ unit in Layer I.

The interplanar distances and the longitudinal and transverse overlap shifts are listed in Table 2. In Layer I, the $Ni(dmit)_2$ units stack in a slightly dimerized fashion, with interplanar distances of 3.58 and 3.67 Å, as is the case for conventional $M(dmit)_2$ salts with closed-shell cations.[1] The arrangement of the $Ni(dmit)_2$ units in Layer I is not clearly influenced by the short Te ⋯ S contacts, compared with that in the conventional $Ni(dmit)_2$ salts with the closed-shell cations. On the other hand, the $Ni(dmit)_2$ units in Layer II stack with an almost uniform interplanar distance (3.57 Å) and with alternate shifts parallel to the longitudinal molecular axis, as is the case for [TTF]-$[Ni(dmit)_2]_2$.[18] This stacking mode is not very common and plays an important role in determining the effective band width and anisotropy of the conduction band. Intermolecular S ⋯ S contacts shorter than the sum of the van der Waals radii (3.60 Å)[19] are observed along the stacking and transverse directions.

The intermolecular overlap integrals among the $Ni(dmit)_2$ LUMOs are listed in Table 3. The electronic band structure of

Table 2 The interplanar distances and 'longitudinal' and 'transverse' overlap shifts in $[Me_3Te][Ni(dmit)_2]_2$ (**1**)

		Interplanar distance/Å	Longitudinal shift/Å	Transverse shift/Å
Layer I	Intradimer	3.58	0.52	1.24
	Interdimer	3.67	2.94	1.08
Layer II	Intradimer	3.57	2.00	0.70
	Interdimer	3.57	2.73	1.27

Table 3 Calculated overlap integrals (S) among LUMOs ($\times 10^{-3}$) for $[Me_3Te][Ni(dmit)_2]_2$ (**1**) (see Fig. 1)

	A	*B*	*p*	*q*	*r*	*t*
Layer I	12.94	−4.59	−1.62	0.49	3.27	−0.03
Layer II	−9.07	−7.91	5.82	0.72	−2.59	

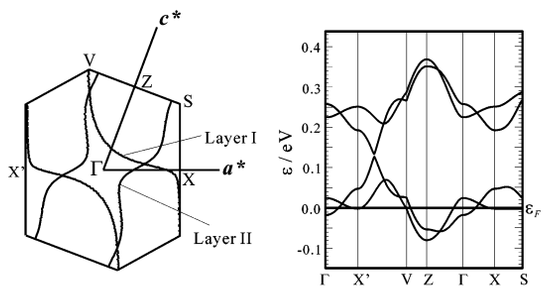

Fig. 3 Calculated band structure and Fermi surface of $[Me_3Te][Ni(dmit)_2]_2$ (**1**).

1 was calculated with the tight-binding approximation. The calculated electronic band structure and Fermi surface are shown in Fig. 3. The three-dimensional calculation confirms that the influence of the interlayer interaction is very small. An interesting point to be noted is that two conduction bands associated with the crystallographically independent layers (I and II) differ from each other in dispersion, degree of filling, and Fermi surface. The intermolecular overlap integrals indicate weak dimerization in Layer II, which reduces the energy gap due to the dimerization and leads to an effectively larger band width. Notably, the interstack interaction, p, that is associated with the Te ⋯ S interaction is enhanced within Layer II. The Fermi surface associated with Layer I is open to the ($\boldsymbol{a}^*$ + $\boldsymbol{c}^*$) direction, and that associated with Layer II is open to the $\boldsymbol{a}^*$ direction. The structural difference between layers I and II results in the dramatic difference in the Fermi surfaces. Both of them are strongly warped and exhibit large deviations from one-dimensionality.

Crystal structure of $[Me_3Te][Ni(dmit)_2]_3{\cdot}(CH_3)_2C(O)$ (2)

The crystal structure of $[Me_3Te][Ni(dmit)_2]_3{\cdot}(CH_3)_2C(O)$ (**2**) is shown in Fig. 4. This salt belongs to the monoclinic system with the space group $P2_1/n$. The crystal structure of **2** is based on a herring-bone arrangement of the $Ni(dmit)_2$ units. The unit cell contains four crystallographically independent $Ni(dmit)_2$ units, two of which are located on the inversion centers. This salt has two crystallographically equivalent $Ni(dmit)_2$ layers, each of which consists of two independent stacks. The $Ni(dmit)_2$ layers are separated from each other by the insulating layers containing the cations and the solvent molecules [Fig. 4(b)]. The averaged formal charge of the $Ni(dmit)_2$ molecule is −1/3 and the $Ni(dmit)_2$ columns have threefold periodicity. Therefore, **2** is considered to be a band insulator.

Four short Te ⋯ S contacts are observed (3.43–3.83 Å), and the Me_3Te^+ cation is surround by four $Ni(dmit)_2$ units. Two of the three $Ni(dmit)_2$ molecules in the repeating unit contact the same Te atom and the space surrounding the remaining $Ni(dmit)_2$ unit is filled with the acetone molecule [Fig. 4(b)]. Even when single crystals of **2** were obtained from a mixture of acetonitrile and acetone (1:1 v/v), only acetone molecules were found in the crystal.

The acetone molecules included in the crystal are accommodated in a channel formed by the $Ni(dmit)_2$ molecules and the Me_3Te^+ cations [Fig. 4(c)]. These acetone molecules can be removed by heating. Preliminary thermogravimetric experiments indicated that the single crystal of **2** begins to release the included solvents at around 30 °C. The weight loss of the polycrystal samples stopped after annealing at 80 °C for 10 min and reached *ca.* 5% *vs.* initial weight, which corresponds to all of the acetone molecules. X-Ray analysis of **2** after annealing also showed that the acetone molecules had been lost. Even after the annealing, the temperature dependence of the resistivity of **2** is unchanged.

Crystal and electronic structures of α-$[MOT][Ni(dmit)_2]_2$ (3)

The crystal structure of α-$[MOT][Ni(dmit)_2]_2$ (**3**) is shown in Fig. 5. This salt belongs to the monoclinic system with the space group $P2_1/c$. The unit cell contains two crystallographically independent $Ni(dmit)_2$ units, each of which forms twin columns interrelated by the 2_1 symmetry. These columns form two crystallographically independent conduction layers (Layer I and II) through intermolecular S ⋯ S contacts. The MOT cations are in contact with both layers through short Te ⋯ S contacts (3.72 and 3.85 Å). These Te ⋯ S contacts enhance the interlayer interaction through short S ⋯ S contacts between the terminal thioxo sulfur atoms.

The interplanar distances and the longitudinal and transverse overlap shifts are listed in Table 4. In both layers, the $Ni(dmit)_2$ units stack almost uniformly (3.55 Å in Layer I and 3.56 Å in Layer II) with alternate shifts parallel to the

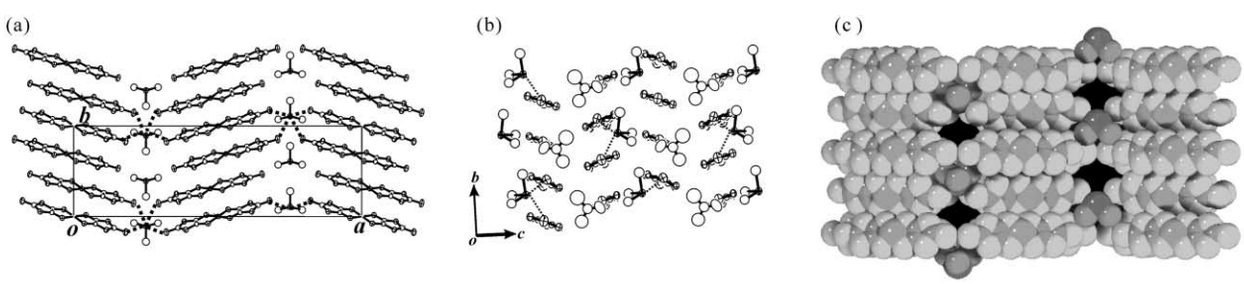

Fig. 4 Crystal structure of $[Me_3Te][Ni(dmit)_2]_3{\cdot}(CH_3)_2C(O)$ (**2**): (a) side view, (b) end-on projection, and (c) space-filling model (acetone molecules are omitted for clarity).

Table 4 The interplanar distances and 'longitudinal' and 'transverse' overlap shifts in α-[MOT][Ni(dmit)$_2$]$_2$ (**3**)

	Interplanar distance/Å	Longitudinal shift/Å	Transverse shift/Å
Layer I	3.55	1.80	0.46
Layer II	3.56	1.83	0.46

Table 5 Calculated overlap integrals (S) among LUMOs ($\times 10^{-3}$) for α-[MOT][Ni(dmit)$_2$]$_2$ (**3**) (see Fig. 5)

	A	*p*	*q*	*r*	*c*
Layer I	−8.10	−0.92	−0.08	1.96	−0.69
Layer II	−8.77	−1.28	0.09	1.20	

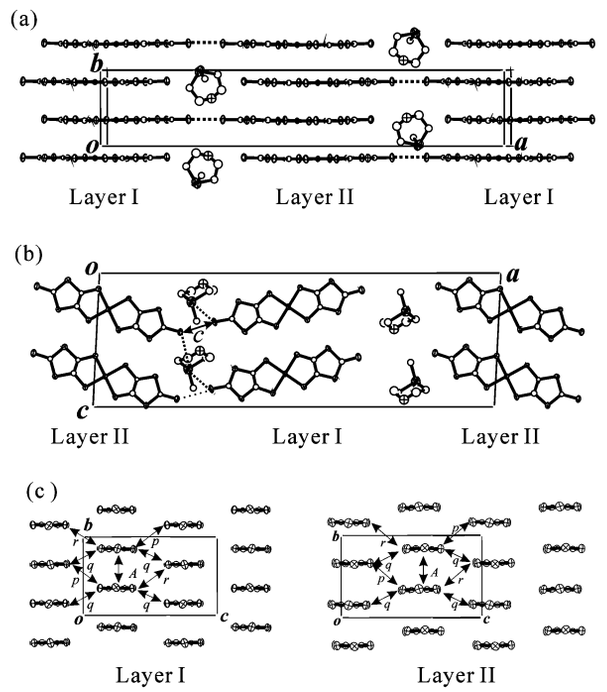

Fig. 5 Crystal structure of α-[MOT][Ni(dmit)$_2$]$_2$ (**3**): (a) side view, (b) top view, and (c) end-on projection of Ni(dmit)$_2$ layers.

longitudinal molecular axis. Short intermolecular S ··· S contacts are observed in all directions, including the interlayer ([100]) direction.

The intermolecular overlap integrals among the LUMOs of the Ni(dmit)$_2$ molecule are listed in Table 5. The calculated electronic band structure and Fermi surface of **3** are shown in Fig. 6. The distinctive feature is the relatively large overlap integral between the conduction layers. The interlayer interaction ($|c|$) is larger than the smallest interaction within the conduction layer ($|q|$). The interaction along the stacking direction ($|A|$) is about 10 times as large as the others. This means that the system is quasi-one-dimensional. The calculated Fermi surface consists of four pairs of planes that are open to the b^* direction. Although three of them are almost flat, indicating strong one-dimensional character, the other exhibits deviation from one-dimensionality. If there were no interlayer interactions, the three pairs of flat planes would become almost degenerate.

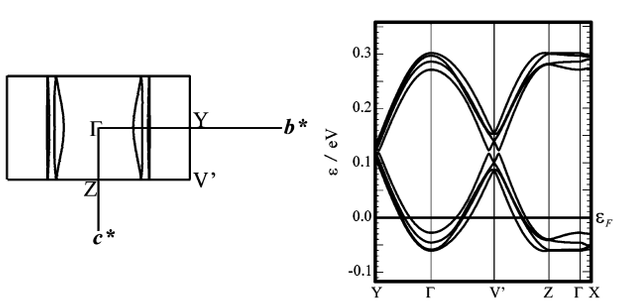

Fig. 6 Calculated band structure and Fermi surface of α-[MOT][Ni(dmit)$_2$]$_2$ (**3**).

Crystal and electronic structures of β-[MOT][Ni(dmit)$_2$]$_2$ (4)

The crystal structure of β-[MOT][Ni(dmit)$_2$]$_2$ (**4**) is shown in Fig. 7. This salt belongs to the monoclinic system with the space group $P2_1/n$. The crystal structure of **4** is based on a herringbone arrangement of Ni(dmit)$_2$ units. The unit cell contains two crystallographically independent Ni(dmit)$_2$ units. The two conduction layers in the unit cell are crystallographically equivalent. The conduction layer consists of two types of Ni(dmit)$_2$ stacks (I and II). The number of short Te ··· S contacts between Stack I and the cation is one (3.81 Å), and between Stack II and the cation it is two (3.81 and 3.83 Å).

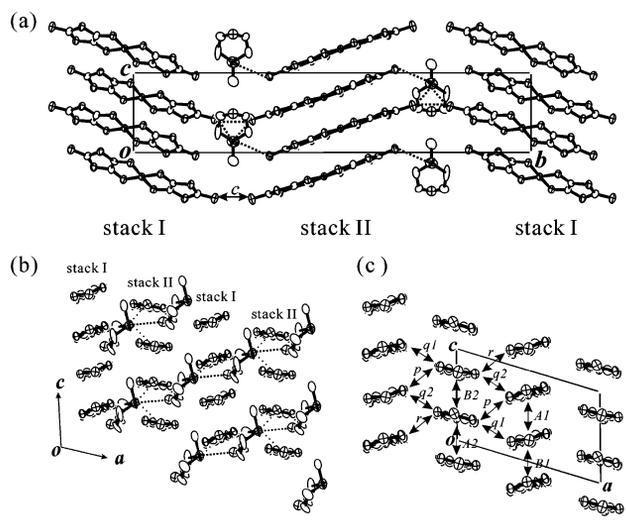

Fig. 7 Crystal structure of β-[MOT][Ni(dmit)$_2$]$_2$ (**4**): (a) side view, (b) end-on projection, and (c) notation of the intermolecular interactions (MOT^+ ions are omitted for clarity).

The interplanar distances and longitudinal and transverse overlap shifts are listed in Table 6. In the conduction layer, the Ni(dmit)$_2$ molecules stack in a dimerized fashion. The interplanar distances for the conventional Ni(dmit)$_2$ salts are about 3.5 Å within a dimer and 3.6–3.7 Å between dimers.[1] In **4**, the intradimer distances are 3.39 (stack I) and 3.44 Å (stack II) and the interdimer distances are 3.73 (stack I) and 3.73 Å (stack II), which means that the degree of dimerization is enhanced.

Notably, a short Te ··· O contact (3.34 Å) is observed between the cations. The cations are connected with each other along the [101] direction to form a one-dimensional supramolecular array. In the ordinary case, a 'hard' oxygen atom coordinates tellurium atom in the highest oxidation state (6+) from its axial direction. In this case, however, the oxygen atom coordinates the tellurium(IV) atom in a lower oxidation state. At present, the driving force for this unusual coordination is not clear.

This one-dimensional cation chain is parallel to the side-by-side direction for the Ni(dmit)$_2$ units. The Te ··· Te repeating distance within the one-dimensional cation chain is 6.24 Å, while the unit cell sizes along the side-by-side direction for the conventional salts suggest that the transverse width of the Ni(dmit)$_2$ unit is about 6.50 Å. The narrow spacing within the rigid supramolecular cation chain together with the short Te ··· S contacts between the cation and the Ni(dmit)$_2$ molecule prevents the Ni(dmit)$_2$ molecules from being aligned

Table 6 The interplanar distances and 'longitudinal' and 'transverse' overlap shifts in β-[MOT][Ni(dmit)$_2$]$_2$ (**4**)

		Interplanar distance/Å	Longitudinal shift/Å	Transverse shift/Å
Stack I	intradimer	3.39	0.61	0.80
	interdimer	3.73	2.96	0.98
Stack II	intradimer	3.44	0.50	0.99
	interdimer	3.73	2.88	0.57

Table 7 Calculated overlap integrals (S) among LUMOs ($\times 10^{-3}$) for β-[MOT][Ni(dmit)$_2$]$_2$ (**4**) (see Fig. 7)

$A1$	17.07
$A2$	19.36
$B1$	−4.74
$B2$	−6.67
p	−0.83
$q1$	−0.03
$q2$	0.76
r	−0.78
c	0.34

with all the molecular planes parallel to the [101] direction (Fig. 7). This suggests that the Te ··· O contact and three Te ··· S contacts provide the Ni(dmit)$_2$ units with suitable conditions for the herring bone arrangement, which gives a clue for the design of supramolecular cation ··· cation contacts with the aim of regulating the arrangement and orientation of anion radicals. The short intermolecular S ··· S contacts are observed in all directions, including the interlayer direction.

The intermolecular overlap integrals among Ni(dmit)$_2$ LUMOs are listed in Table 7. The calculated electronic band structure and Fermi surface are shown in Fig. 8. Due to the

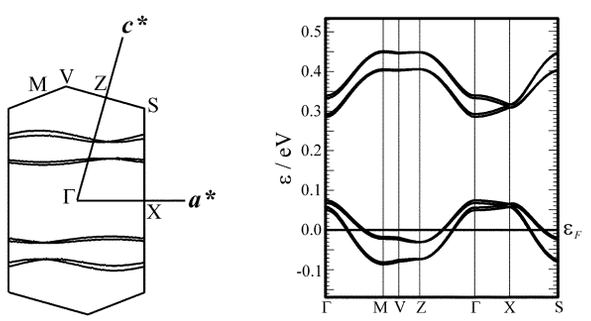

Fig. 8 Calculated band structure and Fermi surface of β-[MOT][Ni(dmit)$_2$]$_2$ (**4**).

strong dimerization, the LUMO band consists of upper (antibonding) and lower (bonding) branches separated by an energy gap. It should be noted that this band splitting due to the dimerization reduces the effective width of the conduction band. When the interlayer interaction is neglected, the Fermi surface consists of *two* pairs of distorted planes, which are associated with two interacting Ni(dmit)$_2$ stacks within the conduction layer. The conduction band is twofold degenerate and the lower branch is effectively half-filled. Introduction of the interlayer interaction removes the degeneracy and leads to the multiple Fermi surface. In this case, each branch associated with the conduction layers slightly deviates from the half-filled state. The system is quasi-one-dimensional along the c^* direction.

Crystal and electronic structures of γ-[MOT][Ni(dmit)$_2$]$_2$ (5)

The crystal structure of γ-[MOT][Ni(dmit)$_2$]$_2$ is shown in Fig. 9. This crystal belongs to the triclinic system with the space group $P\bar{1}$. The unit cell of **5** contains two crystallographically independent Ni(dmit)$_2$ units (A and B) to form a stack in the sequence ··· BAAB ··· with fourfold periodicity.

Table 8 The interplanar distances and 'longitudinal' and 'transverse' overlap shifts in γ-[MOT][Ni(dmit)$_2$]$_2$ (**5**)

	Interplanar distance/Å	Longitudinal shift/Å	Transverse shift/Å
A–A	3.60	0.04	1.34
A–B	3.50	0.36	0.92
B–B	3.76	3.24	1.20

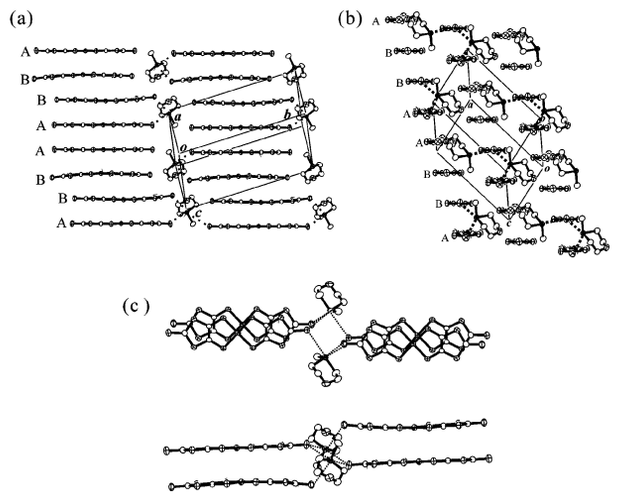

Fig. 9 Crystal structure of γ-[MOT][Ni(dmit)$_2$]$_2$ (**5**): (a) side view, (b) end-on projection, and (c) top view (upper) and side view (lower) of short Te ··· S contacts.

Three short Te ··· S contacts are observed between the cations and the Ni(dmit)$_2$ molecules (3.41, 3.43, and 3.52 Å). In this salt, four Ni(dmit)$_2$ molecules are connected by two MOT cations through short Te ··· S contacts [see Fig. 9(c)]. Therefore, a packing unit in the crystal of **5** consists of one cation and two crystallographically independent Ni(dmit)$_2$ units.

The interplanar distances and the longitudinal and transverse overlap shifts are listed in Table 8. The interplanar distance between the Ni(dmit)$_2$ units A and B is shorter than A–A and B–B distances because the Te ··· S contacts connect A and B within the stack.

Considering that the averaged formal charge of the Ni(dmit)$_2$ unit is −1/2 (corresponding to 1/4 filling of the conduction band) with fourfold periodicity, **5** should be a band insulator.

Character of the Te ··· S contacts

We have obtained some information about the geometry of the Te ··· S contacts. The number of thioxo sulfur atoms that contact the Te atom in the cation ranges from 2 to 4. In many cases, there are 3. In Fig. 10, for four possible sulfur sites (S1, S2, S3 and S4), the distance to the central Te atom increases in the order S1 < S2 < S3, S4. In every case, the shortest contact is located on the opposite side from the alkyl substitution, with R′–Te–S1 angles of 170–180° (this tendency agrees with the definition of the 'secondary bonds'). The angle between the shortest Te ··· S contact and the second shortest one (the S1–Te–S2 angle) ranges from 105 to 120°. The third and fourth contacts exhibit no special tendency.

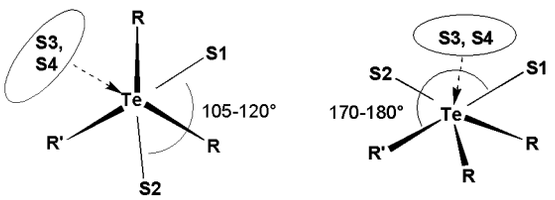

Fig. 10 Top view (left) and side view (right) of the Te ··· S contacts.

Electrical resistivity

The temperature-dependent resistivities of the Ni(dmit)$_2$ salts **1**–**5** are shown in Fig. 11. **2** and **5** exhibit semiconducting behavior. The resistivity values at room temperature ($\rho_{r.t.}$) are 3 (for **2**) and 10 Ωcm (for **5**). The activation energy values (E_a) are 150 (for **2**) and 200 meV (for **5**), respectively. These results are consistent with the prediction that they are band insulators.

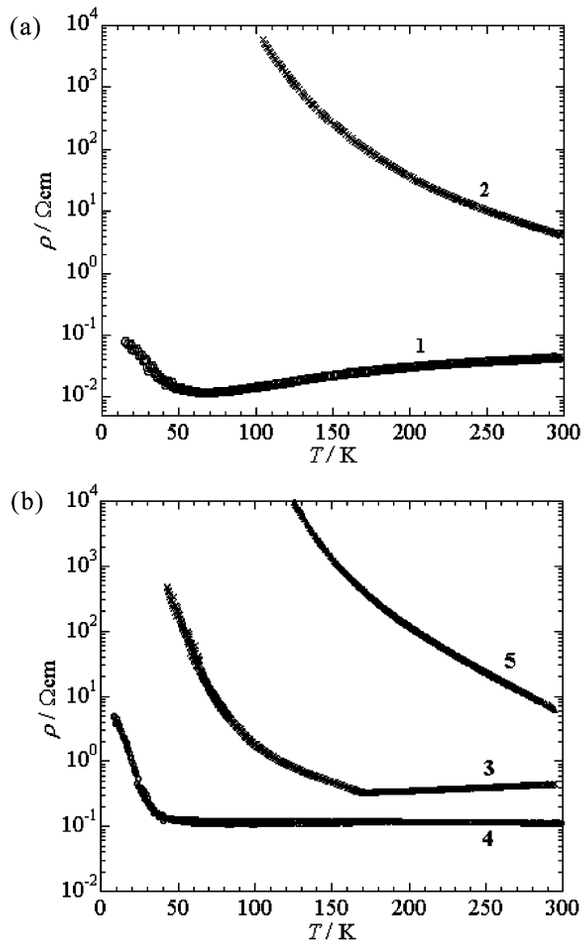

Fig. 11 Temperature dependence of the resistivity of Ni(dmit)$_2$ salts: (a) Me_3Te^+ salts and (b) MOT^+ salts.

The resistivity of **4** is almost temperature independent ($\rho_{r.t.}$ = 0.1 Ω cm) down to about 50 K followed by a moderate increase.

1 and **3** exhibit metallic behavior. The resistivity of **3** ($\rho_{r.t.}$ = 0.4 Ω cm) exhibits a metal–semiconductor transition at 170 K. The resistivity of **1** depends on the quality of the sample. The room temperature resistivity of **1** ranges from 0.04 to 0.2 Ω cm. The resistivity of **1** shows an increase below about 65 K. Lower quality samples (determined by X-ray diffraction photographs) exhibited higher resistivity around room temperature and almost temperature-independent behavior. The transition to the non-metallic state, however, occurred at the same temperature. It should be noted that **1** and **4** remain fairly conductive, even at the lowest temperature measured.

These results are summarized as follows: (1) the band insulators show relatively low $\rho_{r.t.}$ but large E_a (**2** and **5**). (2) When the energy gap due to the dimerization is small (or negligible) and the multiple Fermi surface associated with crystallographically independent conduction layers occurs, the system shows low $\rho_{r.t.}$ values and clearly metallic behavior (**1** and **3**). It should be noted that the number of the metallic Ni(dmit)$_2$-based anion radical salts is still limited. The stability of the metallic state depends on the deviation from one-dimensionality. (3) When the system has an energy band with a large energy gap, due to dimerization, the system shows low and temperature-independent resistivity (**4**). In this case, the interlayer interaction between the crystallographically equivalent conduction layers removes the effectively half-filled state and stabilizes the highly conducting state.

Conclusion

The introduction of two Te-containing cations (Me_3Te^+ and MOT^+) to Ni(dmit)$_2$-based anion radical salts led to a variety of arrangements of Ni(dmit)$_2$ units and high conductivity. X-Ray crystal structure analyses revealed various Ni(dmit)$_2$ arrangements influenced by the short Te ··· S contacts between the cation and the anion. The trialkyltelluronium cations connect the Ni(dmit)$_2$ anion radicals through these Te ··· S contacts and form packing units containing the cations and the anions. These trialkyltelluronium salts can be considered assemblies of these units.

The features of the Te ··· S contacts seems to be correlated with the structural and physical properties as follows: (i) when there are very short Te ··· S contacts (< 3.6 Å) and they connect Ni(dmit)$_2$ units tightly along the stacking direction, the system tends to be a band insulator (**2** and **5**). (ii) When there are Te ··· S contacts that are relatively long but within the sum of the van der Waals radii (from 3.7 to 3.9 Å), they induce novel arrangements of the Ni(dmit)$_2$ units and the system tends to show the highly conducting behavior (**1**, **3**, and **4**).

It should be noted that the Te ··· S contacts, together with the lower molecular symmetry of the cation tend to induce differences in the site potentials and the intralayer interactions between the two crystallographically independent conduction layers in the unit cell, which leads to differences in the band dispersion, the band filling, and the Fermi surfaces (**1** and **3**). The one-dimensional supramolecular array of the MOT^+ ions in **4** promotes the herring-bone arrangement of the Ni(dmit)$_2$ units. In addition, the Te ··· S contact can enhance the interstack interaction (in **1**) and mediate the interlayer S ··· S contact (in **3** and **4**).

In conclusion, the Te(IV)-based cations have the ability to induce novel arrangements of the Ni(dmit)$_2$ units through intermolecular Te ··· S contacts. These results suggest that control of the arrangement of the Ni(dmit)$_2$ anion radical is feasible by tuning with variously shaped cations. The Te(IV)-containing cations will enable further salts to be obtained and thereby lead us to further understanding of the role that the counter cations play in the conducting anion radical salts.

Acknowledgements

This work was partially supported by a Grant-in-Aid for Scientific Research on Priority Areas (No. 10149103 "Metal-Assembled Complexes") from the Ministry of Education, Science, Sports and Culture, Japan.

References

1 (*a*) P. Cassoux, L. Valade, H. Kobayashi, A. Kobayashi, R. A. Clark and A. Underhill, *Coord. Chem. Rev.*, 1991, **110**, 115; (*b*) R.-M. Olk, B. Olk, W. Dietzsch, R. Kirmse and E. Hoyer, *Coord. Chem. Rev.*, 1992, **117**, 99; (*c*) T. Akutagawa and T. Nakamura, *Coord. Chem. Rev.*, 2000, **198**, 297; (*d*) A. E. Pullen and R.-M. Olk, *Coord. Chem.*

Rev., 1999, **188**, 211; (*e*) P. Cassoux, *Coord. Chem. Rev.*, 1999, **185–186**, 213.
2 (*a*) T. Nakamura, H. Tanaka, M. Matsumoto, H. Tachibana, E. Manada and T. Kawabata, *Chem. Lett.*, 1988, **10**, 1667; (*b*) A. S. Dhindsa, J. P. Badyal, C. Pearson, M. R. Bryce and M. C. Petty, *J. Chem. Soc., Chem. Commun.*, 1991, **5**, 322; (*c*) D. M. Taylor, S. K. Gupta, A. E. Underhill and C. E. A. Wainwright, *Thin Solid Films*, 1992, **210/211**, 287; (*d*) A. V. Hughes, D. M. Taylor and A. E. Underhill, *Langmuir*, 1999, **15**, 2477; (*e*) J. Zhai, T.-X. Wei, C.-H. Huang and H. Cao, *J. Mater. Chem.*, 2000, **10**, 625.
3 (*a*) H. Imai, T. Otsuka, T. Naito, K. Awaga and T. Inabe, *J. Am. Chem. Soc.*, 1999, **121**, 8098; (*b*) C. Handrosch, R. Dinnebier, G. Bondarenko, E. Bothe, F. Heinemann and H. Kisch, *Eur. J. Inorg. Chem.*, 1999, **8**, 1259; (*c*) T. Akutagawa, T. Hasegawa, T. Nakamura, S. Takeda, T. Inabe, K.-I. Sugiura, Y. Sakata and A. E. Underhill, *Inorg. Chem.*, 2000, **39**, 2645; (*d*) S. Aonuma, H. Casellas, C. Faulmann, B. Garreau de Bonneval, I. Malfant, P. Cassoux, P. G. Lacroix, Y. Hosokoshi and K. Inoue, *J. Mater. Chem.*, 2001, **11**, 337; (*e*) L. Cronin, S. J. Clark, S. Parsons, T. Nakamura and N. Robertson, *J. Chem. Soc., Dalton Trans.*, 2001, 1347.
4 (*a*) R. Andreu, I. Malfant, P. G. Lacroix, P. Cassoux, K. Roque, E. Manoury, J.-C. Daran and G. G. A. Balavoine, *C. R. Acad. Sci., Ser. IIc: Chim.*, 1999, **2**, 329; (*b*) N. Walker and D. Stuart, *Acta Crystallogr., Sect. A*, 1983, **39**, 158; (*c*) J. Zhai, C. Huang, T.-X. Wei, L. Gan and H. Cao, *Polyhedron*, 1999, **18**, 1513.
5 (*a*) L. Valade, J-P. Legros, M. Bousseau, P. Cassoux, M. Garbauskas and L. V. Interrante, *J. Chem. Soc., Dalton Trans.*, 1985, 783; (*b*) R. Kato, H. Kobayashi, A. Kobayashi and Y. Sasaki, *Chem. Lett.*, 1985, 131; (*c*) H. Kobayashi, R. Kato, A. Kobayashi and Y. Sasaki, *Chem. Lett.*, 1985, 191; (*d*) H. Kim, A. Kobayashi, Y. Sasaki, R. Kato and H. Kobayashi, *Chem. Lett.*, 1987, 1799; (*e*) A. Kobayashi, R. Kato and H. Kobayashi, *Synth. Met.*, 1987, **19**, 635; (*f*) R. Kato, H. Kobayashi, H. Kim, A. Kobayashi, Y. Sasaki, T. Mori and H. Inokuchi, *Synth. Met.*, 1988, **27**, B359; (*g*) R. Kato, H. Kobayashi, A. Kobayashi, T. Naito, M. Tamura, H. Tajima and H. Kuroda, *Chem. Lett.*, 1989, 1839; (*h*) D. Reefman, J. P. Cornelissen, J. G. Haasnoot, R. A. G. de Graaff and J. Reedijk, *Inorg. Chem.*, 1990, **29**, 3933; (*i*) J. P. Cornelissen, E. Müller, P. H. S. Vaassens, J. G. Haasnoot and J. Reedijk, *Inorg. Chem.*, 1992, **31**, 2241; (*j*) A. Miyazaki, A. Izuoka and T. Sugawara, *Bull. Chem. Soc. Jpn.*, 1993, **66**, 2832; (*k*) Y. S. J. Veldhuizen, N. Veldman, A. L. Spek, C. Faulmann, J. G. Haasnoot and J. Reedijk, *Inorg. Chem.*, 1995, **34**, 140.
6 (*a*) E. Canadell, S. Ravy, J. P. Pouget and L. Brossard, *Solid State Commun.*, 1990, **75**, 633; (*b*) E. Canadell, I. E.-I. Rachidi, S. Ravy, J. P. Pouget, L. Brossard and J. P. Legros, *J. Phys. (Paris)*, 1989, **50**, 2967; (*c*) H. Tajima, T. Naito, M. Tamura, A. Kobayashi, H. Kuroda, R. Kato, H. Kobayashi, R. A. Clark and A. E. Underhill, *Solid State Commun.*, 1991, **79**, 337.
7 R. E. Peierls, *Quantum Theory of Solids*, Clarendon Press, Oxford, 1955.
8 (*a*) N. F. Mott, *Metal-Insulator Transitions*, Taylor & Francis, Oxford, 1990; (*b*) E. Canadell, *Coord. Chem. Rev.*, 1999, **185–186**, 629.
9 (*a*) R. Kato, H. Kobayashi, H. Kim, A. Kobayashi, Y. Sasaki, T. Mori and H. Inokuchi, *Chem. Lett.*, 1988, 865; (*b*) H. Kobayashi, R. Kato and A. Kobayashi, *Synth. Met.*, 1991, **41–43**, 2495; (*c*) A. Kobayashi, A. Sato and H. Kobayashi, *J. Solid State Chem.*, 1999, **145**, 564.
10 (*a*) T. Imakubo, H. Sawa and R. Kato, *Synth. Met.*, 1995, **73**, 117; (*b*) T. Imakubo, H. Sawa and R. Kato, *J. Chem. Soc., Chem. Commun.*, 1995, 1667; (*c*) T. Imakubo, T. Maruyama, H. Sawa and K. Kobayashi, *Chem. Commun.*, 1998, 2021; (*d*) T. Imakubo, N. Tajima, M. Tamura, R. Kato, Y. Nishio and K. Kajita, *J. Mater. Chem.*, 2002, **12**, 159; (*e*) B. Domercq, T. Devic, M. Fourmigué, P. Auban-Senzier and E. Canadell, *J. Mater. Chem.*, 2001, **11**, 1570; (*f*) A. S. Batsanov, M. R. Bryce, A. Chesney, J. A. K. Howard, D. E. John, A. J. Moore, C. L. Wood, H. Gershtenman, J. Y. Becker, V. Y. Khodorkovsky, A. Ellern, J. Bernstein, I. F. Perepichka, V. Rotello, M. Gray and A. O. Cuello, *J. Mater. Chem.*, 2001, **11**, 2181.
11 (*a*) N. W. Alcock, *Adv. Inorg. Chem. Radiochem.*, 1972, **15**, 1; (*b*) I. Haiduc, R. B. King and M. G. Newton, *Chem. Rev.*, 1994, **94**, 301.
12 (*a*) V. Farrar and J. M. Gulland, *J. Chem. Soc.*, 1945, 11; (*b*) A. Z. Al-Rubaie, H. H. Al-Shirayda and A. I. Auoob, *Inorg. Chim. Acta*, 1987, **134**, 139.
13 (*a*) H. Poleschner, W. John, G. Kempe and E. Hoyer, *Z. Chem.*, 1978, **18**, 345; (*b*) O. Lindqvist, L. Sjoelin, J. Sieler, G. Steimecke and E. Hoyer, *Acta Chem. Scand., Ser. A*, 1979, **33**, 445.
14 N. Walker and Stuart, *Acta Crystallogr., Sect. A*, 1983, **39**, 158.
15 G. M. Sheldrick, Program for the Refinement of Crystal Structures, University of Göttingen, Germany, 1997.
16 R. Hoffman, *J. Phys. Chem.*, 1963, **39**, 1397.
17 (*a*) T. Mori, A. Kobayashi, Y. Sasaki, H. Kobayashi, G. Saito and H. Inokuchi, *Bull. Chem. Soc. Jpn.*, 1984, **57**, 627; (*b*) M.-H. Whangbo, J. M. Williams, P. C. W. Leung, M. A. Beno, T. J. Emge, H. H. Wang, K. D. Carlson and G. W. Crabtree, *J. Am. Chem. Soc.*, 1985, **107**, 5815.
18 M. Bousseau, L. Valade, J.-P. Legros, P. Cassoux, M. Garbauskas and L. V. Interrante, *J. Am. Chem. Soc.*, 1986, **108**, 1908.
19 A. Bondi, *J. Phys. Chem.*, 1964, **68**, 441.